https://doi.org/10.2352/ISSN.2470-1173.2020.7.ISS-212

Soft-prototyping imaging systems for oral cancer screening

Joyce Farrell[1], Zheng Lyu[1], Zhenyi Liu[2], Henryk Blasinski[1], Zhihao Xu[3], Jian Rong[3], Feng Xiao[3], Brian Wandell[1]

[1]Stanford University, [2]Jilin University, [3]FengYun Vision Technologies

Abstract

We are using image systems simulation technology to design a digital camera for measuring fluorescent signals; a first application is oral cancer screening. We validate the simulations by creating a camera model that accurately predicts measured RGB values for any spectral radiance. Then we use the excitation-emission spectra for different biological fluorophores to predict measurements of fluorescence of oral mucosal tissue under several different illuminations. The simulations and measurements are useful for (a) designing cameras that measure tissue fluorescence and (b) clarifying which fluorophores may be diagnostic in identifying precancerous tissue.

Introduction

Tissue autofluorescence can be used to discriminate between normal and precancerous tissue [1]. This finding has motivated the design and implementation of imaging systems for non-invasive in-vivo measurements of tissue autofluorescence [2].

In most cases, the autofluorescence signal is very weak compared to reflected light. Consequently, one must design special purpose imaging systems that separate the reflected and fluorescent photons. This paper quantifies the autofluorescence signals available for one application - oral cancer detection. We combine knowledge about these signals with image systems simulations to design illuminant and sensor combinations that can help clinicians measure the autofluorescence of oral mucosal tissue and ultimately identify specific signals that are diagnostic of oral cancer.

Related work

Several light-based devices help dentists visualize oral mucosal abnormalities associated with precancerous and cancerous lesions (e.g Velscope®, OralID®, Identafi®). These products use short-wavelength LEDs to excite endogenous fluorophores present in oral mucosal tissue. The clinician wears glasses that block the short-wavelength reflected light from the LED illumination, rendering the middle- and long-wavelength fluorescence signals visible. These devices are designed around the observation that unhealthy tissue has a weak level of fluorescence [1,3-5]. Hence, the physician looks for dark areas on the tongue and in the oral cavity where the fluorescence is absent.

A decrease in certain types of tissue fluorescence is associated with precancerous and cancerous tissue. Many researchers have proposed that changes in endogenous tissue fluorophores are responsible for the decreased fluorescence. For example, some have attributed the decreased fluorescence to a reduction in FAD (flavin adenine dinucleotide), a molecule that plays an important role in cell respiration and metabolism, and to changes in collagen and elastin that occur with cellular damage [6-10].

An increase in other types of tissue fluorescence has been associated with cancer. For example, several investigators have reported an increase in fluorescence caused by NADH (the reduced form of nicotinamide adenine dinucleotide) associated with the progression of cancer [8,11]. Investigators have also detected the distinctive spectral signature of porphyrin fluorescence in cancerous lesions [3,6,12–15]. However, because porphyrin fluorescence is also measured on the dorsal side of healthy tongues [9], porphyrin fluorescence has the potential of producing false-positive outcomes when it is used as a diagnostic for oral cancer in humans [12].

Multiple changes in tissue fluorophores may occur with the progression of cancer, and there may be new discoveries about additional causes of a change in tissue autofluorescence. To build a diagnostic tool we must create an imaging system that separates the effects of these multiple fluorophores. Ultimately through the acquisition of quantitative data about the fluorescent signals from clinical cases, we may be able to implement meaningful diagnostic tools. An early diagnosis of oral cancer can be lifesaving.

The main goal of the work described in this paper is to build a special purpose camera system that can be used to acquire and interpret measurements of tissue fluorescence in the oral cavity. Image systems simulations enable us to explore the relationship between fluorophores, illuminant spectra and fluorescence. We aim to design and build a calibrated camera that can replace the eyes and clinical judgment of the clinician with measurement data that can quantify the amount and type of tissue fluorescence in a large region of the oral cavity. Aggregating these data and monitoring patient outcomes, should enable us to improve oral health predictions.

Image systems simulation

We use image systems simulations to investigate how well fluorescence can be detected as we make different choices of the illuminant spectral power, the camera filters and the sensor color filter array. To perform the simulations, we use the Image Systems Engineering Toolbox for Cameras (isetCam), a freely available, open-source, Matlab toolbox[1]. The software has been described and validated in several other applications [16–18].

We begin by modeling a camera of the type we propose to acquire data and show that the camera model accurately predicts measured sensor responses (RGB values) for both reflective and fluorescent calibration targets. Then we describe simulations of tongue reflectance and the fluorescence of molecules that are known to be present in the healthy oral cavity. The simulations are based on information from the literature that characterize the excitation and emission properties of endogenous tissue fluorophores. We created a second open-source, available Matlab toolbox[2] to document the data and fluorescence computations. Finally, we simulate the design of an illumination source and

[1] https://github.com/iset/isetcam/wiki

[2] https://github.com/iset/isetfluorescence/wiki

camera that can image, detect and quantify the autofluorescent signals from the mouth.

Camera modeling

We model an imaging system that was built by FengYun Vision Technologies to capture reflectance and fluorescence images of the oral cavity. We refer to the imaging system as the "OralEye camera". The camera includes a light source that illuminates oral mucosal tissue with either a broadband spectral (white) LED light or narrowband short wavelength (blue) LED light with peak energy at 385 nm (Figure 1). The two different lights enable the user to measure both tissue reflectance and fluorescence. The image system includes sharp wavelength cut filters that limit the spectrum of the illuminant and allow the sensors to respond mainly to the fluorescence wavebands. The exposure duration and sensor gain can be pre-programmed to use exposure bracketing.

The OralEye camera includes a longpass filter that blocks wavelengths less than 475 nm from reaching the imaging sensor. This filter is necessary because tongue fluorescence is approximately 10,000 times less than the blue light that is reflected from the tongue (see Figure 1). The camera also has a shortpass filter in front of the blue LED lights so that wavelengths greater than 475 nm do not reach the tongue where it would be reflected. Finally, the OralEye camera has an NIR blocking filter to block wavelengths greater than 700 nm.

We can efficiently represent the combined effect of the spectral transmittances of filters and the spectral quantum efficiency of the imaging sensor in a 3xW matrix, S, where W is the number of wavelength samples. This combination represents the spectral quantum efficiency of the whole system (Figure 1c), including the longpass and NIR blocking filters. We use this matrix to predict the raw sensor camera values for spectral radiance input.

Validation

To validate the model, we captured OralEye camera images of a miniature version of a Macbeth Color Checker (MCC) illuminated with the broadband ("white") LEDs using 5 and 10 msec exposure durations and with the uv ("blue") LEDs using a 30 msec exposure duration. All camera images were captured with the same gain and no ambient illumination.

The images shown in Figure 2 represent the sensor RGB values (unprocessed) for the Macbeth ColorChecker captured under two different illuminants. For each camera image, we extracted the mean raw RGB values for the 24 color patches. The rectangle superimposed on each color patch indicates the image area used to calculate the mean R, G and B values for the 24 color patches. The data are stored in a 3x24 target matrix, T.

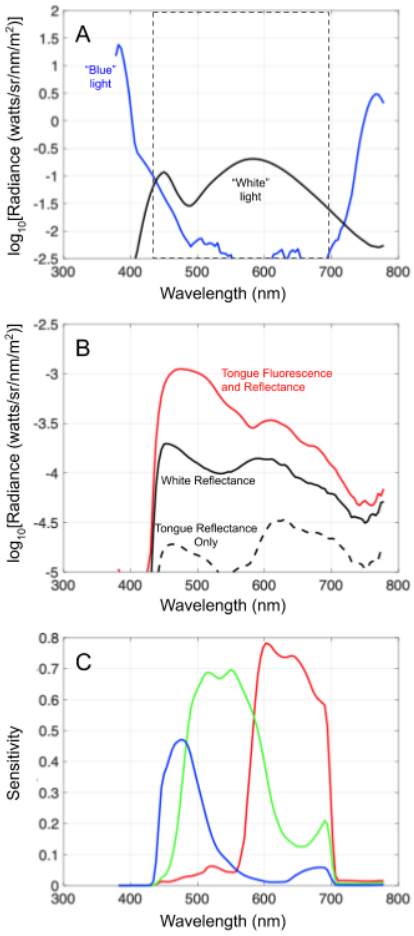

Figure 1. *A) Spectral energy in the short wavelength ("blue") and broadband ("white") LEDs, plotted on in units of log10. The dashed box marks the cutoff frequency of a long pass filter that passes spectral energy greater than 425 nm and a shortpass filter that blocks spectral energy greater than 700 nm. B) Spectral energy measured from a tongue (red line) and a white calibration target (black solid line) using a spectroradiometer equipped with a 425 nm longpass filter. The dashed line plots the tongue reflectance multiplied by the short-wavelength light, representing the expected tongue radiance based on reflectance only. C) Spectral quantum efficiency of the OralEye camera, including the effects of the 425 nm long pass filter and the NIR blocking filter.*

The white broadband illuminant produces RGB values that create a recognizable test chart. The blue UV LED illuminant produces an image in which a few of the diffusely reflecting non-fluorescent surfaces are violet/bluish. Several other surfaces appear orange, brown and green, indicating that these materials have fluorescent pigments. The MCC pigments absorb energy in the UV light and emit energy in the longer wavelengths, like certain biological tissues. Thus, calibrating with respect to this target is a useful approach to validating the camera model with respect to the goal of measuring tissue fluorescence.

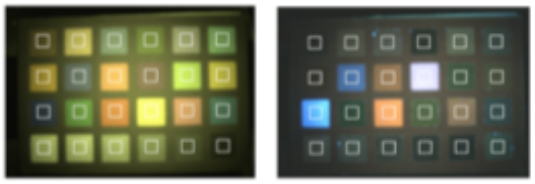

Figure 2. *Raw camera images captured when the MCC is illuminated with the broadband "white" LEDs (shown on the left), and short wavelength "blue" LEDs (shown on the right). The rectangles superimposed on the images indicate the image area over which the mean R, G and B pixel responses were calculated. Many of the patches include fluorescent pigments that are visible when illuminated by the "blue" light. The fluorescence will also be present when illuminated by the "white" LED light, but the number of fluorescent photons is very low compared to the number of reflected photons.*

We used a spectroradiometer (PhotoResearch PR670) to measure the spectral radiance of each of the 24 color patches under these two different lights and stored each set of measurement data in a Wx24 matrix, R. The fluorescence emitted by the MCC pigments illuminated with UV light is four orders of magnitude weaker than the reflected light. Like the OralEye camera, the dynamic range of the PR670 spectroradiometer is not high enough to simultaneously measure both the reflected and fluorescing photons. Hence, we place a longpass filter with a cut wavelength of 425 nm in front of the PR670 to measure the spectral radiance of each of the 24 color patches illuminated with the UV light.

We use the spectral radiance measurements of the MCC color patches (R) and a linear model for the camera sensors (S) to predict the mean MCC RGB camera values (T'). We start with a linear model based on the combined effect of the spectral transmittances of all filters (including the longpass and NIR blocking filters) and the spectral quantum efficiency of the imaging sensor provided by the filter and sensor manufacturers (see Figure 1c).

The predicted raw camera RGB values for each of the 24 color patches illuminated with the two different illuminants are calculated as $T' = S \cdot R$. Figure 3a shows plots the predicted RGB values (T') against the measured RGB values (T) normalized by dividing by exposure duration. Figure 3b shows that it is possible to improve the fit between predicted and measured RGB values by applying a linear affine transformation to the sensor model, S. Figure 3c compares the original sensor model that is based on data from the filter and sensor manufacturers and the improved sensor model based on the linear transformation. This figure illustrates that the improved fit has more crosstalk between the R and B channels and an increased gain in the B channel. There is also a small but insignificant additive term (0.003)

The results shown in Figure 3 confirm that the camera model accurately predicts measured sensor responses (RGB values) for both reflective and fluorescent calibration targets. In the next section of our paper, we combine the camera model with knowledge about the spectral properties of fluorophores in order to evaluate the effect that the spectral energy of the illuminant will have on tissue fluorescence and, consequently, sensor responses.

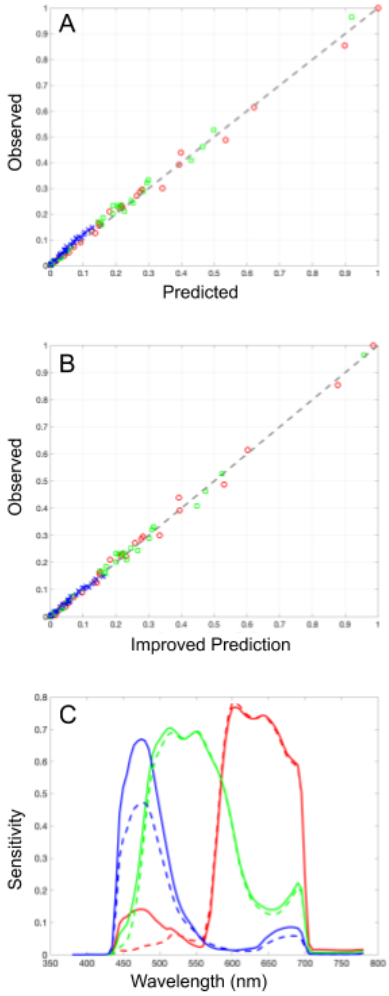

Figure 3*. Predicted and measured camera sensor responses to the Macbeth ColorChecker patches under different lights after accounting for exposure duration. R, G and B values are represented by red, green and blue symbols, respectively. Open circles represent the RGB values for the white light and asterisks represent the RGB values for the ultraviolet (UV) light. The data plotted in the first figure (A) are predicted by the original sensor model-based data provided by the filter and sensor manufacturers. The data plotted in the second figure (B) were obtained by applying a linear transformation of the original sensor model in order to improve the fit between predicted and measured camera RGB values. The figure on the bottom (C) compares the original (dashed lines) and linearly transformed (solid lines) sensor models.*

Fluorophore simulations

The development of light-based oral cancer screening devices were inspired by scientific reports that precancerous (dysplastic) and cancerous tissue fluoresce less than healthy tissue [3,19,20]. The lower fluorescence in cancerous tissue has been attributed to lower concentrations of FAD, collagen and elastin [9,21]. Further work on fluorescence in cancerous tissue suggested that there are higher concentrations of NADH [8,22] and porphyrins [8,22,23]. The opposing effects require us to separately measure the decrease in fluorescence (FAD, collagen and elastin)

from the increase in fluorescence (NADH and porphyrins). We use image systems simulation to assess how well we can separate the effects from these two groups of fluorophores.

Each fluorophore is characterized by an excitation-emission matrix (EEM). The columns of the EEM contain the relative spectral emission for each excitation wavelength. Typically, as observed by Stokes [24], the emissions arise only at wavelengths that are longer (lower energy) than the excitation wavelength; consequently, the EEM is triangular. The EEM is also called the Donaldson matrix.

Biological tissues often contain multiple fluorophores, each with a different EEM. The emissions from this mixture can be calculated by a weighted sum of their separate contributions [25]. We use the spectral energy of the illuminant, the EEM data for NADH, FAD, collagen, elastin and porphyrins (provided by [26]), measured tongue reflectance, and the sensor model to predict the OralEye RGB values (Figure 4).

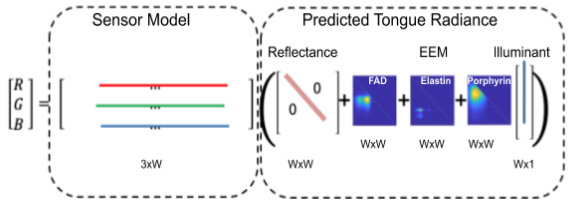

Figure 4: *The simulated OralEye RGB values. The illuminant spectral energy of the 385 nm light multiplies the weighted sum of the fluorophore EEMs plus the tongue reflectance. This calculation generates an expected spectral radiance energy. The OralEye sensor model responds to the radiance to produce the camera RGB values.*

Camera chromaticity coordinates

It is virtually impossible to illuminate the oral cavity uniformly. To reduce the impact of the nonuniform illuminant, we use camera chromaticity responses to estimate the presence of different fluorophores

$$r=R/(R+G+B),\ g = G/(R+G+B)$$

The chromaticity coordinate values are a quantitative measure of the camera response that is invariant with the local illumination level. Figure 5 plots the predicted chromaticity for different concentrations of each of the individual tissue fluorophores. The origin of the line is at the chromaticity of the tongue reflectance. Introducing fluorophores at increasing concentrations shifts the camera chromaticity along a line. As the fluorophore concentration increases, the chromaticity shifts further from the tongue reflectance. The impacts of NADH and collagen on the chromaticity is relatively small compared to FAD and elastin. The small effects of NADH and collagen are explained because their excitation sensitivities do not overlap significantly with the illuminant energy (385 nm). FAD and elastin move along lines in a similar direction making their effects hard to discriminate. The porphyrins are different. The excitation sensitivity of the porphyrins overlaps with the illuminant energy making them bright, and the porphyrin emissions are primarily captured in the R channel.

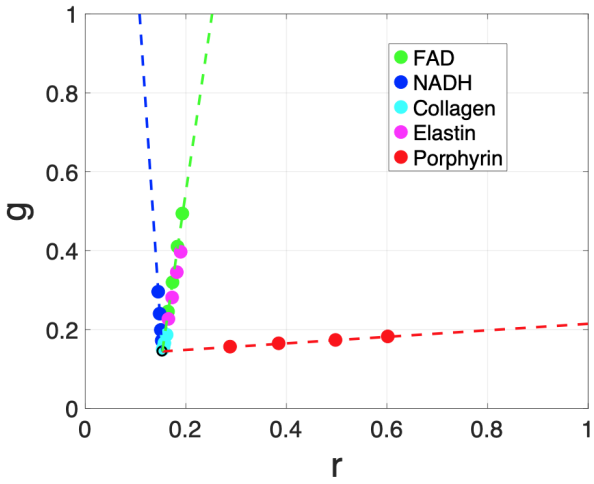

Figure 5: The chromaticity coordinates of the simulated spectral radiance from the tongue for different fluorophores with a range of concentrations. The tongue reflectance under the 385 nm illuminant is shown by the black circle. Simulating increasing concentrations of porphyrins produces an expected camera chromaticity along the red dashed line. Each of the other colored symbols shows the effect of simulating various concentrations of the other fluorophores.

OralEye images

OralEye images captured under 385 nm illumination are shown for three participants (Figure 6, left side). The image appearance is due almost entirely to fluorescence. In the absence of fluorescence, the reflected light intensity would be below the sensitivity limits of the camera. The teeth are very fluorescent, emitting light over many wavelengths. The tongue fluorescence spans a more limited set of wavelengths that is characterized by a limited range of camera image pixel chromaticity coordinates.

For each of the participants we selected a large region within the dorsal aspect of the tongue (white box). The chromaticity coordinates for unprocessed camera image pixels in this region are plotted in the graphs (Figure 6, right side). The tongue chromaticity values span a similar line for the 3 participants shown in Figure 6, as well as other participants not shown here. These camera image pixel chromaticity values span the expected values predicted by combinations of the key tongue fluorophores. The lines showing the expected chromaticity coordinates for separate fluorophores are the same as those in the simulation (Figure 5). In all cases, one end of the chromaticity coordinates approaches the red line corresponding to different concentrations of porphyrins. The other end of the chromaticity coordinates extends past the simulated line for FAD, elastin and collagen, approaching the simulated line for NADH.

Had the data been scattered in chromaticity, it might be difficult to identify a quantitative expectation for healthy participants. Thus far, we collected data from a relatively small number of subjects (10), but the very close agreement in these participants is encouraging. It suggests that we might be able to define a narrow, quantitative expectation for the chromaticity range in the healthy dorsal tongue.

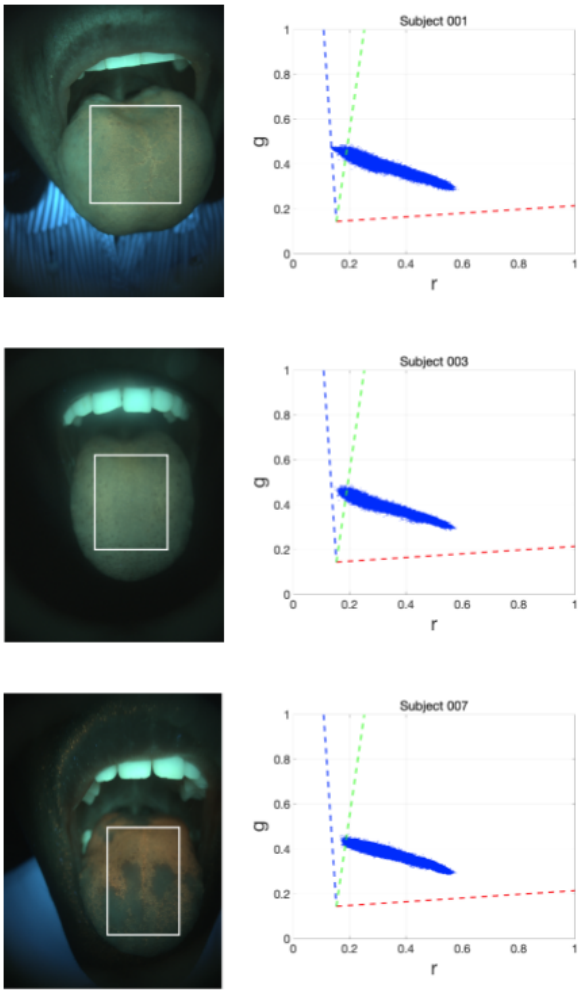

Figure 6: *The camera chromaticity coordinates from three participants measured with the OralEye camera. The images in the left column were captured under the 385 nm illuminant. Despite the very short wavelength, the images contain a wide range of colors that arise from the fluorescence of the tongue, teeth, face and clothing. For each participant we selected two regions of interest and we plot the chromaticity coordinates in those regions in the graphs shown in the right column. The dashed lines are the expected boundaries of the chromaticity coordinates based on fluorophore simulation.*

Discussion

Endogenous fluorophores in biological tissue are widespread and provide an opportunity for non-invasive in-vivo diagnosis of tissue health and pathology [1]. The ability to detect radiance emitted by fluorophores in the mouth may be an important source of information for diagnosing oral cancer. Many investigators have used specialized devices, particularly endoscopes, to measure these signals [2-4, 6-11].

Even using slightly invasive and carefully calibrated radiometric instruments, the exact identity of the fluorophores remains uncertain. The camera simulations confirm that the expected differences in the spectral radiance from some of the tongue fluorophores is small. There is a small separation between the chromaticity from NADH and three fluorophores (FAD, elastin, and collagen). The largest separation is between these fluorophores and the emissions from the porphyrins. The measurements across the surface of the tongue in the participants that we have characterized thus far suggest that the range of measured chromaticity values may be fully characterized as the mixtures of these agents within a small expected range of concentrations.

Summary

We designed and built an imaging system that quantitatively and non-invasively measures fluorescence in the oral cavity. We used image systems simulation to model the response to known oral fluorophores. The measurements from the tongues of healthy participants are consistent with the simulations and suggest that our system can quantify the presence of these fluorophores. The regularity in the measurements across these participants suggests that these measurements may provide a biomarker of the typical fluorophore concentrations in the healthy dorsal tongue.

References

[1] M. Monici, "Cell and tissue autofluorescence research and diagnostic applications," *Biotechnol. Annu. Rev.*, vol. 11, pp. 227–256, 2005.

[2] N. Ramanujam, "Fluorescence spectroscopy of neoplastic and non-neoplastic tissues," *Neoplasia*, vol. 2, no. 1–2, pp. 89–117, Jan. 2000.

[3] A. Gillenwater *et al.*, "Noninvasive diagnosis of oral neoplasia based on fluorescence spectroscopy and native tissue autofluorescence," *Arch. Otolaryngol. Head. Neck Surg.*, vol. 124, no. 11, pp. 1251–1258, Nov. 1998.

[4] P. M. Lane *et al.*, "Simple device for the direct visualization of oral-cavity tissue fluorescence," *Journal of Biomedical Optics*, vol. 11, no. 2. p. 024006, 2006, doi: 10.1117/1.2193157.

[5] M. W. Lingen, J. R. Kalmar, T. Karrison, and P. M. Speight, "Critical evaluation of diagnostic aids for the detection of oral cancer," *Oral Oncol.*, vol. 44, no. 1, pp. 10–22, Jan. 2008.

[6] R. Alfano, D. Tata, J. Cordero, P. Tomashefsky, F. Longo, and M. Alfano, "Laser induced fluorescence spectroscopy from native cancerous and normal tissue," *IEEE J. Quantum Electron.*, vol. 20, no. 12, pp. 1507–1511, Dec. 1984.

[7] R. Drezek *et al.*, "Autofluorescence Microscopy of Fresh Cervical-Tissue Sections Reveals Alterations in Tissue Biochemistry with Dysplasia¶," *Photochemistry and Photobiology*, vol. 73, no. 6. p. 636, 2001

[8] M. G. Müller *et al.*, "Spectroscopic detection and evaluation of morphologic and biochemical changes in early human oral carcinoma," *Cancer*, vol. 97, no. 7, pp. 1681–1692, Apr. 2003.

[9] D. C. G. De Veld, M. J. H. Witjes, H. J. C. M. Sterenborg, and J. L. N. Roodenburg, "The status of in vivo autofluorescence spectroscopy and imaging for oral oncology," *Oral Oncol.*, vol. 41, no. 2, pp. 117–131, Feb. 2005.

[10] I. Pavlova, M. Williams, A. El-Naggar, R. Richards-Kortum, and A. Gillenwater, "Understanding the biological basis of autofluorescence imaging for oral cancer detection: high-resolution fluorescence microscopy in viable tissue," *Clin. Cancer Res.*, vol. 14, no. 8, pp. 2396–2404, Apr. 2008.

[11] I. Georgakoudi *et al.*, "Fluorescence, reflectance, and light-scattering spectroscopy for evaluating dysplasia in patients with Barrett's esophagus," *Gastroenterology*, vol. 120, no. 7, pp. 1620–1629, Jun. 2001.

[12] D. M. Harris and J. Werkhaven, "Endogenous porphyrin fluorescence in tumors," *Lasers Surg. Med.*, vol. 7, no. 6, pp. 467–472, 1987.

[13] F. H. J. Figge, G. S. Weiland, and L. O. J. Manganiello, "Cancer detection and therapy; affinity of neoplastic, embryonic, and traumatized tissues for porphyrins and metalloporphyrins," *Proc. Soc. Exp. Biol. Med.*, vol. 68, no. 3, p. 640, Jul. 1948.

[14] A. M. del C. Batlle, "Porphyrins, porphyrias, cancer and photodynamic therapy—a model for carcinogenesis," *J. Photochem. Photobiol. B*, vol. 20, no. 1, pp. 5–22, 1993.

[15] Y. Yuanlong, Y. Yanming, L. Fuming, L. Yufen, and M. Paozhong, "Characteristic autofluorescence for cancer diagnosis and its origin," *Lasers Surg. Med.*, vol. 7, no. 6, pp. 528–532, 1987.

[16] J. E. Farrell, F. Xiao, P. B. Catrysse, and B. A. Wandell, "A simulation tool for evaluating digital camera image quality," in *Image Quality and System Performance*, 2003, vol. 5294, pp. 124–131.

[17] J. Farrell, M. Okincha, and M. Parmar, "Sensor calibration and simulation," in *Digital Photography IV*, 2008, vol. 6817, p. 68170R.

[18] J. E. Farrell, P. B. Catrysse, and B. A. Wandell, "Digital camera simulation," *Appl. Opt.*, vol. 51, no. 4, pp. A80–90, Feb. 2012.

[19] C. S. Betz *et al.*, "Autofluorescence imaging and spectroscopy of normal and malignant mucosa in patients with head and neck cancer," *Lasers Surg. Med.*, vol. 25, no. 4, pp. 323–334, 1999.

[20] M. Mascitti *et al.*, "An Overview on Current Non-invasive Diagnostic Devices in Oral Oncology," *Front. Physiol.*, vol. 9, p. 1510, Oct. 2018.

[21] R. Richards-Kortum, R. Drezek, K. Sokolov, I. Pavlova, and M. Follen, "Survey of endogenous biological fluorophores," *Handbook of biomedical fluorescence*, pp. 237–264, 2003.

[22] I. Georgakoudi *et al.*, "NAD(P)H and collagen as in vivo quantitative fluorescent biomarkers of epithelial precancerous changes," *Cancer Res.*, vol. 62, no. 3, pp. 682–687, Feb. 2002.

[23] D. R. Ingrams *et al.*, "Autofluorescence characteristics of oral mucosa," *Head Neck*, vol. 19, no. 1, pp. 27–32, Jan. 1997.

[24] G. G. Stokes, "On the change of refrangibility of light," *Philosophical Transactions of the Royal Society of London*, vol. 142, pp. 463–562, Jan. 1852.

[25] H. Blasinski, J. Farrell, and B. Wandell, "Simultaneous Surface Reflectance and Fluorescence Spectra Estimation," *IEEE Transactions on Image Processing*, 2020 (in press).

[26] R. S. DaCosta, H. Andersson, and B. C. Wilson, "Molecular Fluorescence Excitation--Emission Matrices Relevant to Tissue Spectroscopy\P," *Photochem. Photobiol.*, vol. 78, no. 4, pp. 384–392, 2003.

Acknowledgements

We thank Adam Wandell for proposing the project. We thank Rangtao Huang, Kaijun Feng, and Richard Xiao for software development and Tingcheng Zhang for the mechanical and LED board design. And we thank Chris Holsinger and Tulio Valdez for many helpful discussions.

Author Biographies

Joyce Farrell *is the Executive Director of the Stanford Center for Image Systems Engineering and a Senior Research Associate in the Department of Electrical Engineering at Stanford University. She received a doctorate from Stanford in 1981 and has worked at several companies and research institutions, including the NASA Ames Research Center, New York University, the Xerox Palo Alto Research Center and Shutterfly.*

Zheng Lyu *received his M.S. degree in electrical engineering from Stanford University in 2019. He is currently pursuing his Ph.D. degree in electrical engineering with Stanford University. Prior to joining Stanford University, he worked on several projects about optoelectronics at Tsinghua University.*

Zhenyi Liu *received his MS in Electrical Engineering at Ulsan National Institute of Science and Technology, UNIST (2015), Korea. He is currently a PhD candidate in Automotive Engineering at Jilin University, China (2016-present). Zhenyi was a Visiting Student Researcher at Stanford University (2017-2019).*

Henryk Blasinski *received a Ph. D. degree from the Department of Electrical Engineering, Stanford University, CA in 2018. He was a Fulbright Scholar with the Department of Electrical and Computer Engineering, University of Rochester, Rochester, NY, from 2010 to 2011. Henryk is a recipient of the 2014 SPIE Digital Photography X Best Paper Award.*

Zhihao Xu *is expected to receive the B.E. degree in telecommunication engineering from Nanjing University, Nanjing, China, in June 2020. He has been a student intern for Beijing Fengyun Vision Technologies since January 2019 and worked as student intern at the Department of Electrical Engineering of Stanford University from July to August 2019. He will start his doctorate in computational imaging at Tsinghua University in September 2020.*

Jian Rong *is the co-founder and VP of Algorithms at Beijing FengYun Vision Technologies. He received a bachelor's degree from Beijing Institute of Technology. He has worked at several companies, including Agilent Technologies and Vimicro.*

Feng Xiao *is the Founder of Beijing FengYun Vision Technologies and a strategic advisor of the Stanford Center for Image Systems Engineering at Stanford University. He received a doctorate from Stanford and a bachelor's degree from University of Science and Technology of China. Before founding FengYun Vision in 2016, he worked at several companies, including Texas Instruments, Agilent Technologies, Motorola, Fairchild Imaging and Vimicro.*

Brian A. Wandell *is the first Isaac and Madeline Stein Family Professor in the Stanford Psychology Department and a member, by courtesy, of Electrical Engineering, Ophthalmology, and the Graduate School of Education. He is Director of the Stanford Center for Cognitive and Neurobiological Imaging and Deputy Director of the Wu Tsai Neurosciences Institute at Stanford.*

JOIN US AT THE NEXT EI!

IS&T International Symposium on

Electronic Imaging

SCIENCE AND TECHNOLOGY

Imaging across applications . . . Where industry and academia meet!

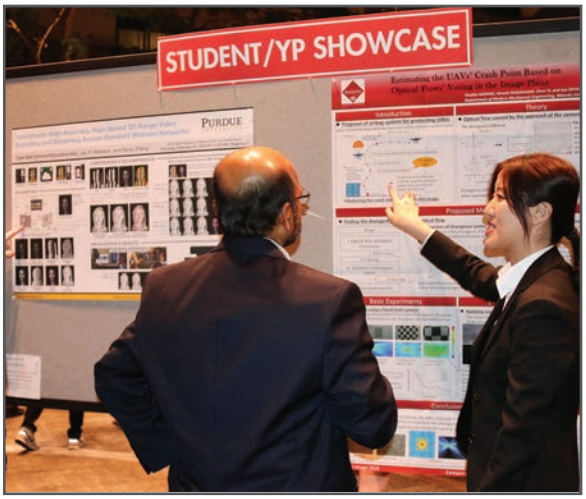

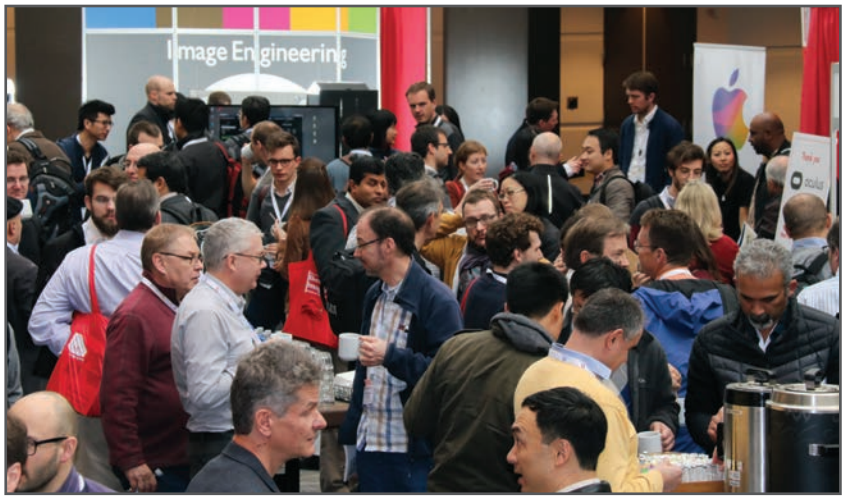

• SHORT COURSES • EXHIBITS • DEMONSTRATION SESSION • PLENARY TALKS •
• INTERACTIVE PAPER SESSION • SPECIAL EVENTS • TECHNICAL SESSIONS •

www.electronicimaging.org

IS&T
imaging.org